

MICROBUNCHING-INSTABILITY-INDUCED SIDEBANDS IN A SEEDED FREE-ELECTRON LASER

Z. Zhang^{1,2}, Y. Ding¹, W. M. Fawley¹, Z. Huang^{1*}, J. Krzywinski¹,
A. Lutman¹, G. Marcus¹, A. Marinelli¹, and D. Ratner¹

¹ SLAC, Menlo Park, CA 94025, USA

² Tsinghua University, Beijing 100084, China

Abstract

The measured spectrum of the soft X-ray self-seeding at the LCLS has a pedestal-like distribution around the seeded frequency, which limits the spectral purity and seeding applications without a post-undulator monochromator. In this paper, we study the origins of the pedestals and focus on the contributions of microbunching instability prior to the FEL undulator. We show that both energy and density modulations can induce sidebands in a seeded FEL. Theory and simulations are used to analyze the sideband content relative to the seeding signal. The results place a tight constraint on the longitudinal phase space uniformity for a seeded FEL.

INTRODUCTION

Many efforts have been devoted to improve the longitudinal coherence and spectral purity of the X-ray free-electron lasers (FELs) since the unequivocal success of existing facilities which are based on the self-amplified spontaneous emission (SASE) [1, 2]. While the relative bandwidth of SASE FELs are limited to at least 10^{-3} or larger, one can decrease the output bandwidth and increase the longitudinal coherence by initiating the FEL process with a coherent seed [3–6], or by imprinting the electron beam with a coherent density modulation (bunching) at the wavelength of interest [7–10]. Under ideal circumstances (high-quality seed of sufficient power and uniform electron beam, etc.), one can obtain completely coherent, high-power X-ray pulses that approach Fourier limit.

However, imperfections of the electron beam or of the seed will reduce the quality of the seeded FEL output [11–14]. In the measurement of self-seeded soft X-ray radiation spectrum at the Linac Coherent Light Source (LCLS) [6], there is often a pedestal-like distribution around the seeded frequency. In the absence of a post-undulator monochromator, this contamination limits the spectral purity and may degrade certain user applications. Further studies have ruled out the possibility that the pedestal-like distributions in the spectra come from the spectrometer noise or the monochromator optics. Microbunching instability growth of the electron beam prior to the undulator, mostly induced by the longitudinal space charge during the long-distance acceleration and drift sections [15, 16] and directly observed at the LCLS recently [17], is identified as the main source for these spectral pedestals. In this paper, we show that both energy and density modulations can induce sidebands in a seeded FEL.

Theory and simulations are used to analyze the sideband content relative to the seeding signal. The results place a tight constraint on the longitudinal phase space uniformity for a seeded FEL.

THEORETICAL ANALYSIS

To understand the basic physics of the pedestals, we consider a two-frequency system: the seed and the sideband. The FEL is seeded by a monochromatic radiation whose frequency is at or near the natural FEL resonant frequency ω_1 and the electron beam initially has a longitudinal long-wavelength modulation at frequency ω_s . We describe the longitudinal phase space of the electron beam with the electron ponderomotive phase $\theta \equiv (k_1 + k_u)z - \omega_1 t$ and normalized energy deviation from resonance $\eta \equiv (\gamma - \gamma_0)/\gamma_0$, where $k_1 (= \omega_1/c)$ and k_u are the wave numbers of the radiation and undulator. We will find the following dimensionless variables to be useful in the analysis:

$$\hat{z} \equiv 2k_u \rho z, \quad (1)$$

$$\hat{\eta} \equiv \frac{\eta}{\rho}, \quad (2)$$

$$a_\nu \equiv \frac{eK[JJ]}{8\gamma_0^2 m c^2 k_u \rho^2} E_\nu, \quad (3)$$

where the normalized frequency $\nu = 1 + \Delta\nu \equiv \omega/\omega_1$ and $\nu = 1$ is the resonant frequency. K is the normalized field of the undulator and $[JJ]$ is the Bessel function factor. With these dimensionless variables, the pendulum equations of the two-frequency system can be written as

$$\frac{d\theta}{d\hat{z}} = \hat{\eta}, \quad (4)$$

$$\frac{d\hat{\eta}}{d\hat{z}} = a_1 e^{i\theta} + a_s e^{i\nu\theta} + c.c., \quad (5)$$

$$\frac{da_1}{d\hat{z}} = -b_1, \quad (6)$$

$$\frac{da_s}{d\hat{z}} + i\Delta\nu a_s = -b_s, \quad (7)$$

with the bunching parameters at the seed and the sideband frequency

$$b_1 \equiv \langle e^{-i\theta} \rangle, \quad (8)$$

$$b_s \equiv \langle e^{-i\nu\theta} \rangle. \quad (9)$$

The subscript "1" denotes the variables of the seed and "s" the sideband, respectively. We also introduce the collective

* zrh@slac.stanford.edu

momentum as

$$p_1 \equiv \langle \hat{\eta} e^{-i\theta} \rangle, \quad (10)$$

$$p_s \equiv \langle \hat{\eta} e^{-i\nu\theta} \rangle. \quad (11)$$

Initial Energy Modulation

Let us first consider an initial beam energy modulation: $A(s) = A_0 \cos(k_s s) = \frac{\Delta\gamma}{\gamma} \cos(k_s s)$. Using the scaled energy variable, we have

$$\hat{\eta}_0 = \frac{\hat{A}}{2} e^{i\Delta\nu\theta} + \text{complex conjugate}, \quad (12)$$

where the normalized modulation amplitude $\hat{A} = A_0/\rho$ and $k_s = \omega_s/c$ is the wave number of the modulation.

With the assumptions that $|a_s| \ll |a_1|, |b_s| \ll |b_1|$ and $|p_s| \ll |p_1|$, we can obtain the equations of the field amplitudes as

$$\frac{d^3 a_1}{d\hat{z}^3} \approx i a_1, \quad (13)$$

$$\frac{d^3 a_s}{d\hat{z}^3} + i\Delta\nu \frac{d^2 a_s}{d\hat{z}^2} \approx i\nu a_s + \nu^2 \hat{A} p_1. \quad (14)$$

Eq. (13) is the FEL cubic equation with the solution as

$$a_1(\hat{z}) = \sum_{l=1}^3 D_l e^{-i\mu_l \hat{z}}, \quad (15)$$

where $D_{1,2,3}$ are the coefficients determined by the initial conditions and $\mu_{1,2,3}$ are the roots of the cubic equation

$$\mu_1 = 1, \quad \mu_2 = \frac{-1 - \sqrt{3}i}{2}, \quad \mu_3 = \frac{-1 + \sqrt{3}i}{2}. \quad (16)$$

If we consider the high-gain regime ($\hat{z} \gg 1$), $a_1(\hat{z})$ takes the simple form of

$$a_1(\hat{z}) = D_3 e^{-i\mu_3 \hat{z}}. \quad (17)$$

Equation (14) is an inhomogeneous ordinary differential equation of a_s . If we assume $|\Delta\nu| < \rho$ (i.e., the sideband frequency shift is small compared to the FEL gain bandwidth), the sideband equation is simplified to

$$\frac{d^3 a_s}{d\hat{z}^3} \approx i a_s + i\hat{A} D_3 \mu_3^2 e^{-i\mu_3 \hat{z}}. \quad (18)$$

The solution for the inhomogeneous equation in the high-gain regime with $a_s(0) = 0$ is

$$a_s(\hat{z}) = -\frac{i\hat{A}D_3}{3} \hat{z} e^{-i\mu_3 \hat{z}} = -\frac{i\hat{A}}{3} \hat{z} a_1. \quad (19)$$

Thus the power ratio between the sideband and the seed radiation along the undulator is

$$\frac{P_s(\hat{z})}{P_1(\hat{z})} = \frac{\hat{A}^2}{9} \hat{z}^2 = \frac{(2k_u \rho z)^2}{9} \frac{A_0^2}{\rho^2}. \quad (20)$$

Eq. (20) applies to either lower or upper sideband with a frequency shift much less than the FEL gain bandwidth. The full treatment of this problem, valid for an arbitrary sideband frequency and also at FEL start-up, has been worked out by Lindberg [18].

We note that the ratio of the sideband power vs. the seed power grows quadratically with z and A_0 . This can be understood qualitatively as follows. The energy modulation generates periodic local energy chirp along the electron beam $h(s) = h_0 \cos(k_s s)$. Together with the undulator R_{56} , the seed frequency or phase ϕ will be modulated according to

$$\frac{d\phi(s)}{ds} \sim h(s) R_{56} k_1 = h(s) 2k_u z. \quad (21)$$

This phase modulation generates two lowest sidebands that have field amplitude proportional to h_0 (A_0) and z . If we take the seeding saturation at $2k_u \rho z = 9$, Eq. (20) stated that $A_0 < \frac{1}{3}\rho$ in order for the sideband to not exceed the seed power at saturation. Using the LCLS soft x-ray self-seeding parameters given in Table 1, this leads to $A_0 < 1$ MeV and is a very stringent requirement on the residual energy modulation at the undulator entrance.

Finally the single-frequency sideband analysis can be generalized to broadband sidebands driven by microbunching instability as

$$\frac{P_s(\hat{z})}{P_1(\hat{z})} = \frac{\hat{A}^2}{9} \hat{z}^2 = \frac{(2k_u \rho z)^2}{9} \int_0^{\Delta s} \frac{A(s)^2}{\rho^2} \frac{ds}{\Delta s}. \quad (22)$$

Here $A(s)$ is the energy centroid along the bunch coordinate s , and Δs is the bunch length of a flattop current profile.

Initial Density Modulation

The above analysis can be applied in a straightforward manner to modulations in current. Let us introduce an initial bunching parameter at the sideband frequency $\omega_s = \Delta\nu\omega_1$:

$$b_0 = \langle e^{-i\Delta\nu\theta} \rangle. \quad (23)$$

The sideband field equation for $\Delta\nu = \omega_s/\omega_1 < \rho$ becomes

$$\frac{d^3 a_s}{d\hat{z}^3} \approx i\nu a_s + i\nu a_1 b_0. \quad (24)$$

Similar to Eq. (20), the power ratio between the sideband and the seeding signal is

$$\frac{P_s(\hat{z})}{P_1(\hat{z})} = \frac{b_0^2}{9} \hat{z}^2 = \frac{(2k_u \rho z)^2}{9} b_0^2, \quad (25)$$

which also grows quadratically with the initial density modulation amplitude and the undulator length.

Combining Eqs. (14) and (24), we obtain the sideband driven by both energy and density modulations (the terms with \hat{A} and b_0 , respectively). Nevertheless, the typical residual density modulation is much smaller than the residual energy modulation (in units of ρ). For the microbunching instability, density and energy modulations are 90° out of

phase. In this case, the existence of the density modulation increases the lower sideband at the expense of upper sideband power and keeps the total sideband content approximately constant. Thus, the density modulation modifies the spectral pedestal shape without increasing the total spectral energy in the pedestals.

1-D SIMULATION

To verify the previous analytical considerations, we have numerically solved the time-dependent 1-D FEL equations for a number of initial modulation conditions to study the growth of the sideband power. Here we use the parameters of the soft X-ray self-seeding FEL experiment settings at the LCLS in Table 1. In the simulation, the electron beam is ideal with uniform current distribution and vanishing slice energy spread. The seed power distribution is also uniform. The energy modulations are added to the electron beam with cosine form with various periods and amplitudes. The modulation wavelength is $2 \sim 10 \mu\text{m}$, which is the range of the microbunching instability observed in the experiment [17]. The modulation amplitude ranges from 0.1 MeV to 0.6 MeV, and the corresponding \hat{A} is within 0.03 to 0.2.

Table 1: Simulation Parameters in 1-D FEL Code

Parameter	Value	Unit
Beam energy E	3.48	GeV
Slice energy spread	0	MeV
Normalized emittance ϵ_N	0.9	μm
Current I	1.4	kA
Average β	30	m
Undulator period λ_u	3	cm
FEL parameter ρ	8.6×10^{-4}	
Gain length L_G	1.6	m
Seeding wavelength λ_r	2.29	nm
Seeding power	20	kW
Energy modulation wavelength	2-10	μm
Energy modulation amplitude	0.1-0.6	MeV

The total field amplitude a and the bunching factor at the seed frequency b_1 for different energy modulation amplitudes are given in Fig. 1. The FEL reaches saturation around $\hat{z} = 9$. The total power of the FELs, which is proportional to a^2 , is maintained while we increase the energy modulation amplitude. However, the bunching factor b_1 is reduced near the saturation at large modulation amplitude.

The FEL spectra along the undulator are shown in Fig. 2 to illustrate the growth of the sideband power. The spectra are normalized by the power of the seed ($\Delta E = \hbar\omega_s$). There are two sideband peaks near the seed and their power ratios increase along the undulator. The difference between the lower and upper sideband peaks is due to the shape of the gain curve in FELs. The lower sideband has larger gain. It is also noted that when the first-order sideband becomes large enough, the second-order one will appear with larger energy offset. Here

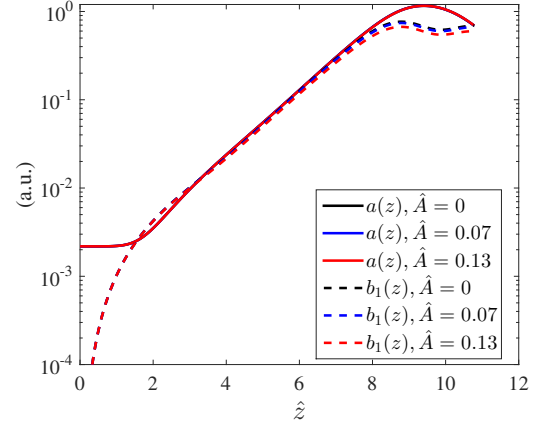


Figure 1: The total field amplitude a and bunching factor b_1 along the undulator with various energy modulation amplitude \hat{A} .

we only consider the first-order sideband as the second-order are always very small in our cases of interest.

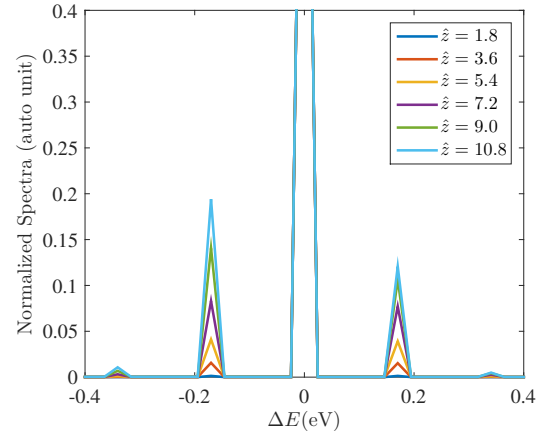


Figure 2: The spectra along the undulator length to illustrate the growth of the sideband power. The spectra are normalized by the power of the seed. The modulation wavelength is $8 \mu\text{m}$ and amplitude is $\hat{A} = 0.13$.

First we study the energy offset of the sideband peaks to the seed, as shown in Fig. 3. The energy offset of the two sideband peaks are the same and proportional to the inverse of the modulation wavelength. Simulation results show that the energy offset is independent of the modulation amplitude and undulator length.

To get the growth rate of the sideband power, we plot the power ratios of the lower sideband to the seed along the undulator for different modulation amplitudes in Fig. 4. The theoretical analysis predicts that the sideband power ratio grows quadratically with \hat{z} and \hat{A} (see Eq. 20) in the high-gain regime. We fit the simulation results at $\hat{z} > 1$ in Fig. 4 with second-order expressions of \hat{A} and \hat{z} . The fitting coefficients of the curves are all around $\frac{1}{9}$ as predicted in the theory, which verifies the previous analysis.

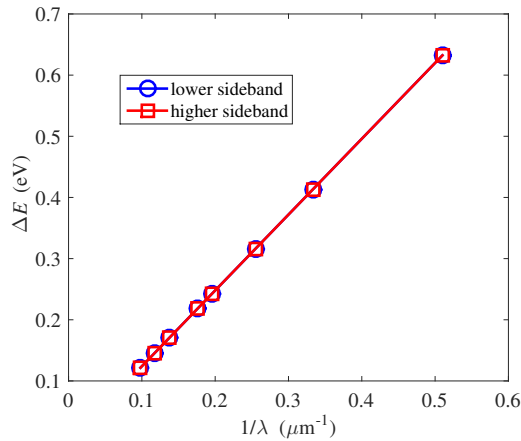


Figure 3: The energy offset of the sideband peaks to the seed versus the inverse of the modulation wavelength.

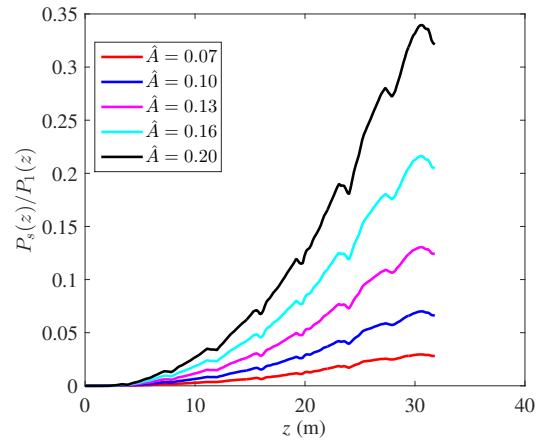


Figure 5: The ratio of the lower sideband to the seed along the undulator for different modulation amplitude in Genesis simulations.

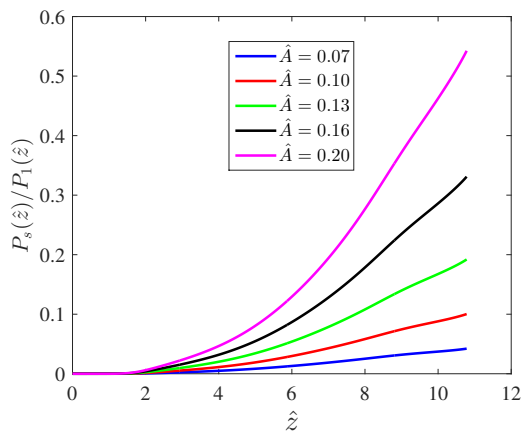


Figure 4: The ratio of the lower sideband to the seed along the undulator for different modulation amplitude.

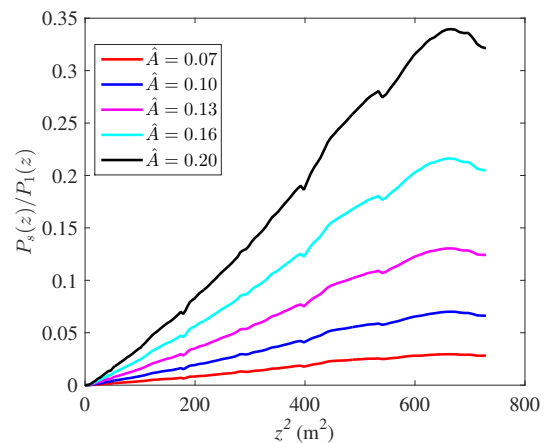


Figure 6: The ratio of the lower sideband to the seed versus the square of the undulator length (after removing the drifts) for different modulation amplitude in Genesis simulations.

3D GENESIS SIMULATIONS

3D Genesis [19] simulations were also performed to validate the theory and 1D simulations. We adopt similar parameters with the 1D simulations, but include the drifts between undulator sections. The energy offset of the sidebands are the same as found previously in the 1D simulations in Fig. 3. The power ratio along the undulator are shown in Fig. 5.

It can be seen that the power ratio of the sideband to the seed has a small drop at the beginning of new undulator sections in the Genesis simulations. This is because the upstream drift length matches the seed frequency and produces additional phase shifts (mismatches) for the sidebands. If we remove the drifts in the plot and use the square of the undulator length in Fig. 6 as the scale, the power ratio grows quadratically with the undulator length and modulation amplitude, which is consistent with the theory and 1D simulations.

SUMMARY

In this paper, we have investigated the effects of residual energy and density modulations on the output of a seeded FEL. A simple 1D theory is developed to estimate the sideband content and agrees well with simulations. The power ratio of the sidebands to the seeded signal grows quadratically with the modulation amplitude and undulator length before FEL saturation. Further work includes detailed comparison with the experimental observations and developing methods to produce a more uniform electron beam in the longitudinal phase space.

ACKNOWLEDGMENT

We thank C.-X. Tang and E. Allaria for useful discussions. This work was supported by U.S. Department of Energy Contract No. DE-AC02-76SF00515.

REFERENCES

- [1] P. Emma *et al.*, Nat. Photonics 4, 641 (2010).
- [2] T. Ishikawa *et al.*, Nat. Photonics 6, 540 (2012).
- [3] J. Feldhaus, E. Saldin, J. Schneider, E. Schneidmiller, and M. Yurkov, Opt. Commun. 140, 341 (1997).
- [4] G. Geloni, V. Kocharyan, E. Saldin, Journal of Modern Optics 58, 1391 (2011).
- [5] J. Amann *et al.*, Nat. Photonics 6, 693 (2012).
- [6] D. Ratner *et al.*, Phys. Rev. Lett. 114, 054801 (2015).
- [7] L. H. Yu, Phys. Rev. A 44, 5178 (1991).
- [8] G. Stupakov, Phys. Rev. Lett. 102, 074801 (2009).
- [9] E. Allaria *et al.*, Nat. Photonics 6, 699 (2012).
- [10] E. Allaria *et al.*, Nat. Photonics 7, 913 (2013).
- [11] W. Fawley and G. Penn, Sincrontrone Trieste tech. note ST/F-TN-06/07 (2006).
- [12] A. Lutman *et al.*, J. Phys. A: Math. Theor. 42, 085405 (2009).
- [13] B. Ji *et al.*, Phys. Rev. ST Accel. Beams 13, 060701 (2010).
- [14] A. Marinelli *et al.*, Phys. Rev. ST Accel. Beams 13, 070701 (2010).
- [15] E. L. Saldin *et al.*, Nucl. Instrum. Methods Phys. Res. Sect. A 490, 1 (2002).
- [16] Z. Huang *et al.*, Phys. Rev. ST Accel. Beams 7, 074401 (2004).
- [17] D. Ratner *et al.*, Phys. Rev. ST Accel. Beams 18,030704 (2015).
- [18] R. Lindberg, ANL tech. note AOP-TN-2015-028 (2015).
- [19] S. Reiche, Nucl. Instrum. Methods A 429, 243 (1999).